

PCCP

Accepted Manuscript



This is an *Accepted Manuscript*, which has been through the Royal Society of Chemistry peer review process and has been accepted for publication.

Accepted Manuscripts are published online shortly after acceptance, before technical editing, formatting and proof reading. Using this free service, authors can make their results available to the community, in citable form, before we publish the edited article. We will replace this *Accepted Manuscript* with the edited and formatted *Advance Article* as soon as it is available.

You can find more information about *Accepted Manuscripts* in the [Information for Authors](#).

Please note that technical editing may introduce minor changes to the text and/or graphics, which may alter content. The journal's standard [Terms & Conditions](#) and the [Ethical guidelines](#) still apply. In no event shall the Royal Society of Chemistry be held responsible for any errors or omissions in this *Accepted Manuscript* or any consequences arising from the use of any information it contains.

Cite this: DOI: 10.1039/xxxxxxxxxx

Received Date
Accepted Date

DOI: 10.1039/xxxxxxxxxx

www.rsc.org/journalname

Molecular organization in freely suspended nano-thick 8CB smectic films. An atomistic simulation.

Mattia Felice Palermo,^a Luca Muccioli,^{a,b} and Claudio Zannoni^{*a}

We present an atomistic molecular dynamics simulation of freely suspended films of the smectic liquid crystal 8CB formed by $n_l = 2, 3, \dots, 10, 20$ theoretical monolayers, determining their orientational and positional order as a function of the film thickness. We find that films are always composed by bilayers of antiparallel molecules, and that in the case of odd n_l , the system prefers to self-assemble in $(n_l + 1)/2$ bilayers, with an increase of surface tension with respect to even n_l samples. We also show that external layers have higher positional and orientational order, and that upon heating the disordering of the system proceeds from the inside, with the central layers progressively losing their smectic character, while the external ones are more resistant to temperature changes and keep the film from breaking.

1 Introduction

One of the most fascinating and intriguing properties of liquid crystals (LC) is their having features somehow intermediate between those of disordered isotropic liquids and those of three dimensional crystals endowed with positional and orientational order. Thus, assuming that each mesogenic molecule can be considered as a rigid rod-like object with position \mathbf{r} and orientation Ω (e.g. given by three Euler angles $\alpha\beta\gamma^1$), the probability $P(\mathbf{r}, \Omega)$ of finding a molecule at a certain position-orientation will be proportional to a constant, the density ρ , in a liquid, to an orientational probability $P(\Omega)$ in a nematic LC, to a periodic function in one dimension $P(z, \Omega)$ in a layered smectic A (SmA), and to a fully three dimensionally periodic function $P(\mathbf{r}, \Omega)$, belonging to some space group, in a crystal.

The student textbook picture of a SmA is that of an infinite regular stack of fluid layers with molecular preferred orientation (the director \mathbf{n}) orthogonal, on average, to the layers and behaving as a 2D fluid in each layer. Other categories of smectic LC exist, where molecules are tilted (smectic C) or where some local positional order around a given molecule (typically hexagonal), rather than decaying exponentially as expected in a liquid, or surviving at arbitrary long distances like in an ideal 2D crystal, decays with a slow, inverse power law of distance²⁻⁴ behaviour (smectic B, SmB). This idealized picture is directly touching upon some fundamental aspects of the statistical mechanics

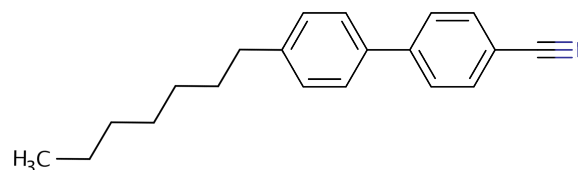


Fig. 1 Molecular structure of 4-n-octyl-4'-cyanobiphenyl (8CB).

of condensed phases, for instance the possibility of existence of a truly infinite order of the layer stacks in 1D and the nature of a 2D fluid and its crystallization⁵. As for the 2D fluid nature of the layer, even when the director is perpendicular to the layers, as in a SmA, the situation is far from obvious. The first issue is: what is the layer constituted of? The simplest answer would be of single molecules, so that the layer spacing would correspond to a molecular length^{6,7} (with due allowance for molecular flexibility⁶⁻¹¹), but this is not necessarily so, e.g. if the molecules have a strong head-to-tail interaction, because of hydrogen bonds¹²⁻¹⁴ or dipoles, and they form quasi dimer pairs¹⁵. As it turns out, this is the case for what is arguably the most well studied smectic LC i.e. 8CB (4-n-octyl-4'-cyanobiphenyl, see **chemical structure in Figure 1**), where a number of X-ray investigations^{16,17} and atomistic computer simulations^{11,18-20} have shown that its smectic phase is strongly interdigitated (smectic A_d , SmA_d) and that its structure is similar, in a way, to a stack of bilayers composed of antiparallel pairs of molecules.

In the case of 8CB the X-ray layer spacing is $d \approx 31 \pm 1$ Å^{11,16,17,21} as compared to a molecular length of ≈ 20 Å. The

^a Dipartimento di Chimica Industriale "Toso Montanari" and INSTM, Università di Bologna, Viale Risorgimento 4, IT-40136 Bologna, Italy; E-mail: claudio.zannoni@unibo.it

^b Laboratoire de Chimie des Polymères Organiques, UMR 5629, University of Bordeaux, Avenue Pey-Berland 16, 33607 Pessac, France

simple 2D fluid picture is further challenged by experimental^{22,23} and simulation¹¹ results concerning 8CB dynamics. Indeed in the ideal 2D fluid model corresponding to a stack of independent layers we would expect the diffusion coefficient for molecular movements inside the layer, D_{\perp} , to be much larger than that from one layer to the next, D_{\parallel} . In reality both measurements and simulations obtain for bulk 8CB $D_{\parallel} > D_{\perp}$, hinting at a situation where layers are far less independent 2D systems than expected, even if different smectic mesogens actually show the expected behaviour^{24,25}.

The possibility offered by smectic LCs of forming thin freely suspended films composed of a small controlled number of layers^{26–28} has prompted a variety of elegant and detailed experimental investigations of layering in smectics and of the nature of their phase changes, as well of their similarity with transitions of 2D or 3D type as the number of layers increases^{29–41}. While these investigations are extremely useful and informative, very little has been done to examine the problem at the molecular level providing insight on the arrangement of molecules and quantifying local and overall positional and orientational order parameters^{42,43}. Obtaining this level of detail represents an important objective that is not easy to achieve experimentally, given the nanometric dimensions of the involved samples and the relatively delicate nature of the films.

From the computational point of view, only a preliminary report on the atomistic simulation of 8CB thin films has appeared but with a very small (64) number of molecules and a non validated force field⁴⁴. Here we wish to tackle the problem with state of the art molecular dynamics simulations. We have chosen 8CB, that has been well investigated experimentally, and for which we have already validated a reliable force field¹⁰ and we have simulated thin films with a number of monolayers varying from 2 to 20 determining their molecular organization. In the next section we describe the modelling and atomistic simulations performed and we discuss our results.

2 Computational Details

We have modelled a thin freely suspended film as an orthogonal sample with a $L \times L$ square section and thickness h . In real experiments the film is suspended across a round, or square as here, aperture a few mm wide²⁷, making the use of periodic boundary conditions around the sides of our nano-sized film entirely appropriate. Along the z axis, where the finite thickness of the film is of course relevant, we augmented the simulation cell with a sufficiently thick vacuum layer above and below the film (see Figure 2), so as to enable the use of periodic boundary conditions in the three dimensions. This setup requires testing that no significant interaction is present between replicas along the z axis. **We thus computed the system energy as a function of the separation between replicas and** found that a vacuum layer of 50 Å thickness was sufficient to ensure the absence of spurious interactions between periodic images.

We have performed a series of NVT (constant number of molecules N , volume V and temperature T) molecular dynamics simulations of films containing a fixed number of 8CB molecules ($N = 1500$ in most cases) adjusting the cell cross section so as

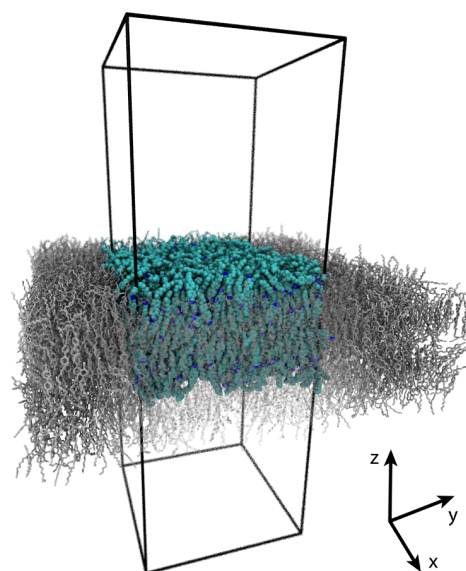


Fig. 2 Snapshot of a $n_l = 2$ film within the simulation box. Light blue molecules represent the original sample while greyed out ones are periodic replicas on the 2D plane. **The laboratory frame axis system is also drawn.**

to obtain thin films of different thickness and correspondingly change the number of layers. The 8CB molecules were modelled at United Atom (UA) level of detail, where hydrogen atoms are embedded in the nearest carbon, so that CH, CH₂, CH₃ groups are treated as suitably parameterized spherical interaction sites, using the previously described modified AMBER-OPLS force field^{45,46}. Simulations were run using the molecular dynamics engine NAMD⁴⁷ with multiple time step integration: bonded, van der Waals, and electrostatic interactions have been calculated every 2, 4 and 4 fs, respectively. **The samples were kept at constant temperature through a thermostat⁴⁸. The choice of the thermostat is always difficult, but fortunately it can affect only the dynamic properties of the system (i.e. the velocity distribution and e.g. the diffusion rates and coefficients) and not the static ones^{48,49}. In addition to that, the differences between different thermostats vanish at increasing system size and should be negligible for our samples given the large number of molecules (at least $N = 1500$ with 22 atoms each). Since we will not discuss any dynamic properties in this paper, we thus opted for the computationally efficient velocity rescaling method⁴⁸.** The Particle Mesh Ewald (PME) method⁵⁰ was used to evaluate long range electrostatic interactions.

To obtain systems with a controlled number of smectic layers, we adjusted the side length L of the cell accordingly to the approximate relation: $n_l \approx NA_{mol}/L^2$. Here, n_l is the desired number of single layers, which we will simply name “layers” from now on and A_{mol} is the cross section area occupied by a 8CB molecule at the film surface. The determination of A_{mol} was carried out on a $n_l = 12$ sample through a trial and error procedure where small variations of L were imposed to find the value that maximizes the height of smectic peaks in the linear density profile, with the re-

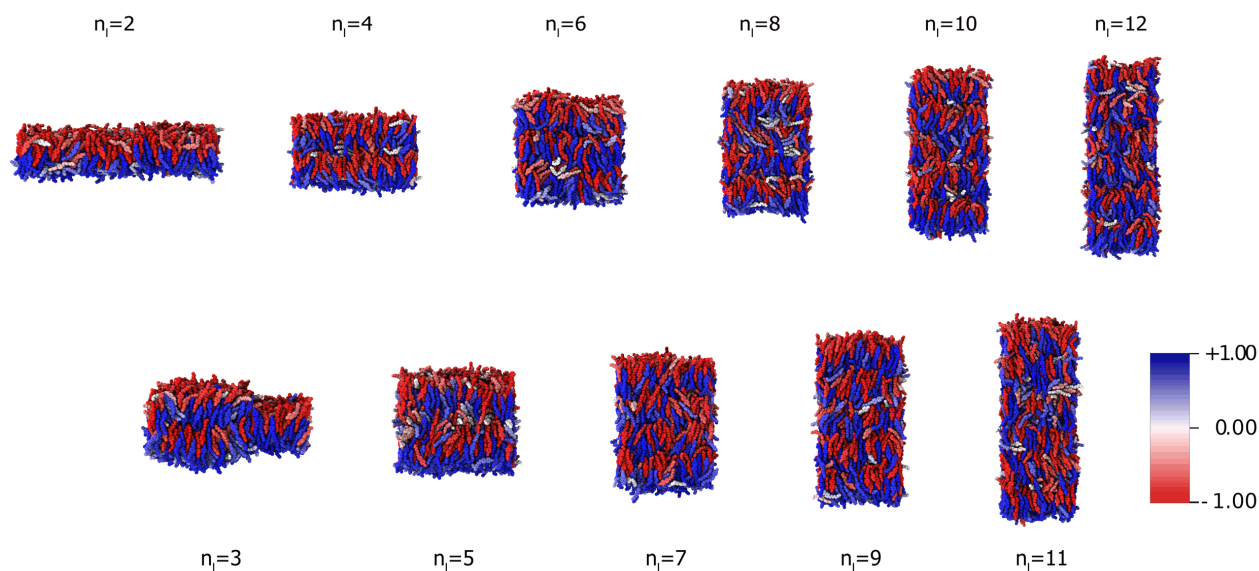


Fig. 3 Typical equilibrated configurations at 300 K of 8CB films with different number of monolayers n_l . Molecules are color-coded according to the value of $\cos \beta_i$, with β_i the angle of the CN axis with respect to the sample director. Red and blue molecules point in opposite direction.

sult $A_{mol} \approx 30.8 \pm 2 \text{ \AA}^2$, that we assume as a basis to calculate the lateral side of our cell for all films. For the $n_l = 12$ layers sample this corresponds to a lateral side of 62 \AA . *NVT* simulations at $T = 300 \text{ K}$ were then run for systems with $n_l = 2 - 12$, including also samples featuring an odd theoretical number of layers n_l (see Figure 3). **Samples were built starting from the system with the largest lateral side and applying an isotropic pressure to the cell in order to obtain films with increasing n_l .** Each simulation was run for at least 100 ns of production time after an equilibration stage of at least 50 ns. An additional series of *NVT* simulations on a $n_l = 12$ sample with temperatures ranging from 300 to 325 K was run to study the effect that the finite thickness has on the 8CB phase transitions.

Finally, one further, much larger, system composed of $N = 12000$ 8CB molecules ($n_l = 20$, $L = 136 \text{ \AA}$) was simulated to verify the existence and extent of positional order variations generated by the two vacuum interfaces as the size increases.

3 Results and discussion

We first report in Figure 3 some typical equilibrium configurations for the films with a different number of monolayers. We see clearly that the molecules self-assemble into antiparallel double layers, making a bilayer the natural unit of film thickness. The case of an odd number of monolayers is interesting, as it could in principle provide a ferroelectricity coming from the excess of dipoles in one direction. This does not prove to be the case, as already observed using SHG spectroscopy in the pioneering work of Hsiung and Shen³³. Indeed we observe that **when the number of layers is odd, and therefore** the number of molecules is intermediate between the optimal one for forming $(n_l - 1)/2$ and $(n_l + 1)/2$ bilayers, $(n_l + 1)/2$ bilayers are always found. In the case of $n_l = 3$, where no inner bilayers can form, we find that regions with one and two bilayers coexist. **Having the coexistence of different number of bilayers instead of the formation of an**

additional bilayer can be rationalized by considering the deviation from the optimal number of molecules per bilayer in samples with odd n_l . In the systems were an additional bilayer is formed, the average number of molecules per bilayer is lower than the one expected in a perfect bilayer. As n_l increases, the lack of molecules decreases and thus it is easier to form an extra layer. The crossover between coexistence and the formation of an extra layer occurs from $n_l = 3$ to 5 in our simulations. In the following section we shall characterize in detail the ordering and structure of the films.

3.1 Positional order

At temperatures below 306.6 K, bulk 8CB is known to form a smectic phase called SmA_d , characterized, as mentioned before, by the presence of bilayers composed by two interdigitated layers of molecules that are oriented in antiparallel directions to optimize the interactions between the strong axial dipoles of these polar molecules.

For a layered phase such as the SmA_d one, the structural periodicity can be expressed in terms of the positional order parameters τ_n ^{51,52}, coefficients in a Fourier expansion of the probability density $P(z)$ of finding a molecule at position z :

$$P(z) = \frac{1}{d} + \frac{2}{d} \sum_{n=1}^{\infty} \tau_n \cos(q_n z) = \frac{\rho(z)}{\rho_0} \cdot \frac{1}{d} \quad (1)$$

where d is the layer spacing, $q_n \equiv 2\pi n/d$ and $\tau_n \equiv \langle \cos(q_n z) \rangle$ is the n th order parameter, $\rho(z)$ is the density profile and ρ_0 is the average density. The smectic phase of 8CB is normally described in terms of the first order τ_1 parameter only, which we will generically refer to as τ , while higher order terms, more difficult to obtain experimentally, are usually neglected.

At an interface with vacuum or air, 8CB molecules align homeotropically exposing their alkyl chains outside the

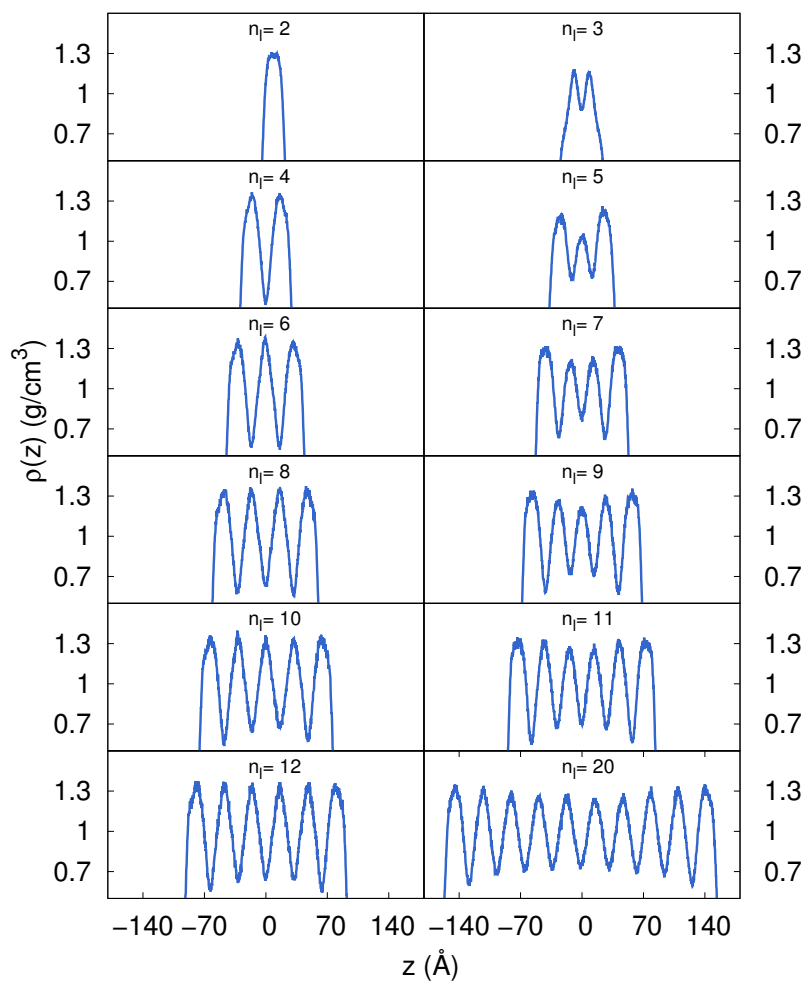


Fig. 4 Density profiles $\rho(z)$ along the z axis for samples ranging $n_l =$ from 2 to 20.

film^{33,53–55}. The homeotropic arrangement of molecules minimizes the number of aromatic cores exposed to the surface and the loss of attractive interactions with the neighbours, while the increased conformational freedom of the chains when not confined by the neighbors allows an entropy gain. In these very thin films the analogous alignment at both surfaces promotes the formation of layers along the direction perpendicular to the surfaces across the whole sample. Real smectic films show considerable oscillations in the density profile along this direction, and usually a higher positional order parameter at the interface compared to the bulk phase⁵⁶. Our results are essentially consistent with these experimental findings, as we can see from Figure 4, where we show the density profiles **computed from the center of mass of the molecules** along the direction normal to the interface for all samples. It can be observed that for each film only a $n_l/2$ (even n_l) or a $(n_l + 1)/2$ (odd n_l) number of peaks is present since, as already mentioned, the films are actually constituted by bilayers and not monolayers, similarly to the bulk. We also notice that the density oscillation for the two external bilayers exposed directly to the vacuum is higher compared to the internal ones. For systems with even n_l , the decay of oscillations towards the center of the film can be observed exclusively for the minima of density profiles, while the maxima remain substantially constant for all the films with n_l up to 12 layers. Conversely, a decreasing trend also for the maxima can be found for the 20 layer film (Figure 5).

In Table 1 we report the local values of τ for the bilayers of each film, which were determined by measuring the projection on the y axis of the distance between maxima and minima of each peak in $\rho(z)/\rho_0$. Values of τ found in thin films are overall higher than those of the bulk at the same temperature ($\sim 20\%$). Moreover, the highest values of τ are found for the external bilayers in all samples. For systems with even n_l only a minimum lowering of positional order is found for the internal layers, which is instead more pronounced in systems with odd n_l .

The average bilayer width d for each film was computed by dividing the film thickness h by the number of bilayers, and is reported in Table 2. The film thickness has been determined from the position on the z axis of the two interfaces with vacuum, measured exploring the surface with a scanning probe ending with a cubic tip of 3 Å. It can be observed that the spacing d for films with even n_l is closer to the values found in our simulations of bulk 8CB¹¹ and higher than the one found for films with odd n_l . A similar value for the bilayer spacing is found by measuring the distance between changes of sign in the profiles of the first rank orientational order parameter $P_1(z)$ to be discussed later (Figure 8).

We have also determined the width of individual couples of bilayers, reported in Table 2. Widths of the inner bilayers have been measured from the distance between the two minima of each peak in the $\rho(z)$. The width of outer bilayers has instead been calculated from the difference between the film thickness h and the total width of inner bilayers. It can be seen that for samples with even n_l the bilayer width is approximately constant throughout the film. On the other hand, external bilayers of films with odd n_l feature a width which is always higher than the one of inner bilayers.

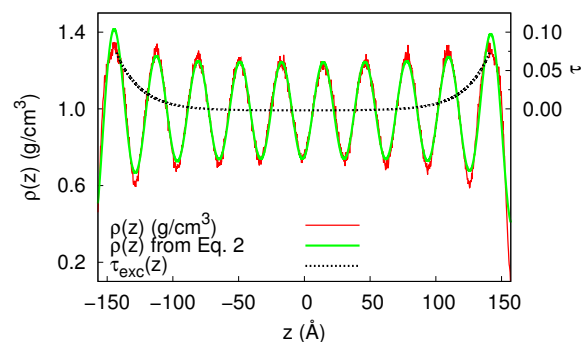


Fig. 5 Fit with Eq. 2 of the density profile along the z axis for the $n_l = 20$ layer film through Equation 2. The dashed black line represents the excess of τ as a function of the distance from the center of the sample.

While density profile oscillations of bulk systems can be accurately described by Equation 1, this is not the case for thin films, as in these systems the order parameter is not constant through the sample. Picano et al.³⁷ proposed a model where the variation of positional order is explicitly taken into account with an excess term τ_{exc} :

$$P(z) = \frac{1}{d} + \frac{2}{d} \sum_{n=1}^{\infty} [\tau_n^{exc}(z) + \tau_n^c] \cos(q_n z), \quad (2)$$

where the surface-induced excess has been written as:

$$\begin{aligned} \tau_{exc}(z) &= \tau(z) - \tau_c \\ &= \frac{\tau_{surf}}{\cosh\left(\frac{h}{\sqrt{2}\xi}\right)} \cosh\left(\frac{\sqrt{2}z}{\xi}\right). \end{aligned} \quad (3)$$

with ξ being the correlation length, h the film thickness and τ_c the smectic order parameter for the bulk of the film, where the surface-induced order is negligible. Here, two assumptions are made: the first is that the positional order decays exponentially and symmetrically moving away from the interface, as imposed by the hyperbolic cosine term (recalling that $\cosh = \frac{1}{2}(e^x + e^{-x})$), and the second is that the studied film is thick enough to have a central region where the surface-induced order is not significant.

Unfortunately it was not possible to fit the density profile $\rho(z)$ using Equation 2 on the smaller $N = 1500$ samples, probably because their thickness is comparable to or shorter than the correlation length ξ . We then attempted to fit the $\rho(z)$ of our largest sample ($N = 12000$, $n_l = 20$). In Figure 5 we report the normalized density profile of this sample together with the fit performed through Equation 2 and the trend of $\tau_{exc}(z)$. Even in this case, the fitting function reproduces only approximately the amplitude of $\rho(z)$ oscillations. The density profile of the two outmost bilayers is in fact overestimated. It can also be seen that the minima and maxima of the density oscillation are not symmetric, the former decreasing more steeply than the latter. This behaviour cannot be

Table 1 Positional order parameter τ_l measured from the projection of the distance between maxima and minima of each peak on the y axis in $\rho(z)/\rho_0$ profiles, for systems with even and odd n_l . n_{bl} is the number of actual bilayers observed in the film. Bilayers placed symmetrically with respect to the centre are numbered progressively from $l = 1$ for the innermost ones to $l = n_b l/2$ if n_{bl} is even and to $l = (n_{bl} - 1)/2$ if it is odd. The central bilayer in samples with odd n_l is numbered with $l = 0$.

n_l	n_{bl}	$\tau_{l=0}$	$\tau_{l=1}$	$\tau_{l=2}$	$\tau_{l=3}$	$\tau_{l=4}$	$\tau_{l=5}$
4	2		0.20				
5	3	0.08	0.13				
6	3	0.19	0.18				
7	4		0.12	0.16			
8	4		0.18	0.18			
9	5	0.12	0.16	0.17			
10	5	0.16	0.17	0.18			
11	6		0.14	0.17	0.17		
12	6		0.17	0.18	0.18		
20	10		0.13	0.14	0.15	0.17	0.18

Table 2 Layer spacing d_l for systems with even and odd n_l . d_l for the inner bilayers has been measured from the distance between the two minima of each peak in the $\rho(z)$ profiles. d_l for the outer bilayers, marked with an asterisk in the table, has been determined from the difference between the film thickness and the width of inner bilayers. n_{bl} is the number of actual bilayers observed in the film. Bilayers placed symmetrically with respect to the centre are numbered progressively from $l = 1$ for the innermost ones to $l = n_b l/2$ if n_{bl} is even and to $l = (n_{bl} - 1)/2$ if it is odd. The central bilayer in samples with odd n_l is numbered with $l = 0$. The film thickness h from the position on the z axis of the two interfaces with vacuum, measured using a scanning-cube algorithm with a tip of 3 Å. The average bilayer width d is computed from the thickness h divided by the actual number of bilayers in the film.

n_l	n_{bl}	$d_{l=0}$ (Å)	$d_{l=1}$ (Å)	$d_{l=2}$ (Å)	$d_{l=3}$ (Å)	$d_{l=4}$ (Å)	$d_{l=5}$ (Å)	h (Å)	d (Å)
4	2		33.2*					66.5	33.2
5	3	22.6	32.2*					82.1	27.4
6	3	32.1	32.2*					96.5	32.2
7	4		26.6	30.5*				114.1	28.5
8	4		32.2	32.2*				128.8	32.2
9	5	27.5	28.3	30.4*				144.9	29.0
10	5	32.2	31.9	32.3*				160.6	32.1
11	6		28.3	29.1	31.2*			177.1	29.5
12	6		31.9	31.9	32.3*			191.9	32.0
20	10		32.0	31.5	31.8	31.2	32.7*	318.2	31.8

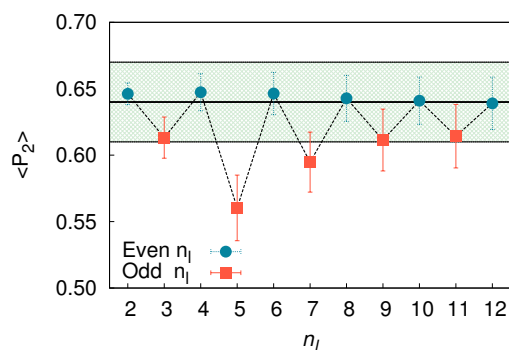


Fig. 6 Average second rank order parameter ($\langle P_2 \rangle$) as a function of the number of theoretical layers in the film. The black line corresponds to the bulk average ($\langle P_2 \rangle$) within its standard deviation (blue dotted area) for a sample of 750 molecules¹¹.

accounted for by Equation 2, as the cosine term oscillates symmetrically around the mean value of density. Additionally, Equation 2 considers the layer spacing to be constant and independent of the distance of the interface, while for our model this is not the case. Nevertheless, through this exercise we were able to estimate the correlation length ξ from the surface as being of the order of magnitude of a few nanometers (~ 3 nm, with τ_{surf} set to 0.18 - see Eq. 3).

3.2 Orientational order

To determine the overall degree of orientational order in 8CB films we have calculated the second moment of the single molecule orientational distribution, usually referred to as $\langle P_2 \rangle$. This order parameter has been computed building and diagonalizing a ordering matrix \mathbf{Q} ⁵⁷:

$$\mathbf{Q}(t) = \frac{1}{2N} \sum_{i=1}^N [3\hat{u}_i(t) \otimes \hat{u}_i(t) - \mathbf{I}], \quad (4)$$

where \hat{u}_i is the chosen reference molecular axis, in our case the principal inertial axis of the molecule, and \mathbf{I} is the identity matrix. Instantaneous values of P_2 for each configuration are obtained by taking the largest eigenvalue of the \mathbf{Q} matrix. This scalar is then averaged over the production trajectory to obtain an overall sample order $\langle P_2 \rangle$. In Figure 6 and in Table 3 we report the values of $\langle P_2 \rangle$ as a function of the number of layers in the sample. For systems with even n_l , it can be seen that $\langle P_2 \rangle$ does not depend on the number of layers and essentially coincides with the value found in bulk (horizontal black line). Samples with an odd number of layers n_l instead always show a lower order parameter, that upon increasing n_l approaches the bulk value from below. The system with $n_l=3$ needs once more a special mention, as it consists of two distinct regions featuring one and two bilayers each contributing to a higher order, comparable to samples with an even n_l .

A better understanding of the orientational order in these smectic thin films can be obtained by studying how it is related to the peculiar spatial organization across the film. With this purpose, we report in Figure 7 the trend of the local orientational order

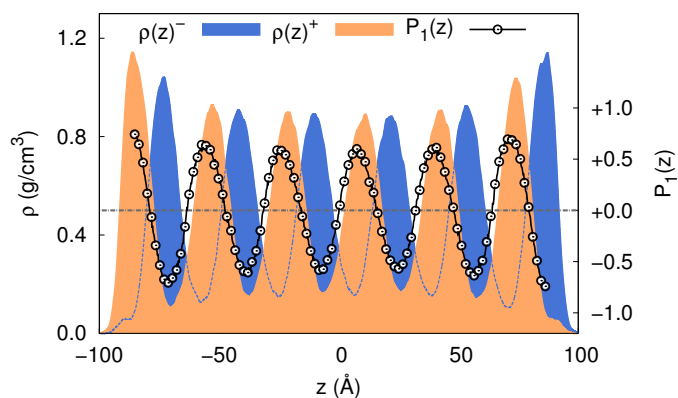


Fig. 8 Density profiles of the layers $\rho(z)^{\pm}$ and polar order parameter $P_1(z)$ as a function of z for the $n_l = 12$ sample.

along the layer normal, $P_2(z)$:

$$P_2(z) = \frac{3}{2} \langle (\hat{u}_i \cdot \hat{z})^2 \rangle - \frac{1}{2} \quad (5)$$

where \hat{u}_i is the reference axis of the i th molecule belonging to a virtual layer at a distance z from the surface, while \hat{z} is the normal to the surface, in this case coinciding with the phase director. It can be seen in Figure 7 that the orientational order varies along z , and that the profile resembles the one observed for the density $\rho(z)$ in the smectic phase, with each peak of the order parameter corresponding to the bilayer center, while a steep decrease is observed for the interstitial region between two adjacent layers. For systems with even values of n_l up to 12, no relevant dependence of the peak height on the number of layers is observed, resulting in the constant trend of $\langle P_2 \rangle$, previously shown in Figure 6, while for the larger $n_l = 20$ sample, inner layers show a slightly lower orientational order compared to the external ones.

Samples with odd n_l exhibit lower peaks for the internal layers or no peaks at all in the case of $n_l=5$ layers (Figure 7). As the sample thickness increases, the disorder originating from the excess of molecules can, as noticed before, be better distributed among the layers and therefore we observe gradually higher internal peaks, thus the increasing trend of the average order parameter observed in Figure 6. Again, the system with $n_l=3$ is an exception to this trend and features a value of $\langle P_2 \rangle$ higher than expected in the center of the film and a lower value at the surface.

More details about the arrangement and the pairing of cyanobiphenyls across the film can be obtained from the first rank order parameter profiles along the normal to the interface $P_1(z) = \langle \hat{u}_i \cdot \hat{z} \rangle$. This profile is reported in Figure 8 for the $n_l = 12$ sample, together with the density profiles of the individual layers $\rho(z)^-$ and $\rho(z)^+$, corresponding to molecules with $P_1 > 0$ or < 0 , respectively. It can be seen that each change of sign of $P_1(z)$ is located in correspondence of the positions z at which $\rho(z)^+$ and $\rho(z)^-$ cross. It is also evident from the density profile that peaks corresponding to the outside layers facing vacuum are much taller than their inner counterparts, suggesting the presence of a net surface dipole moment at the film surface. This hypothesis can

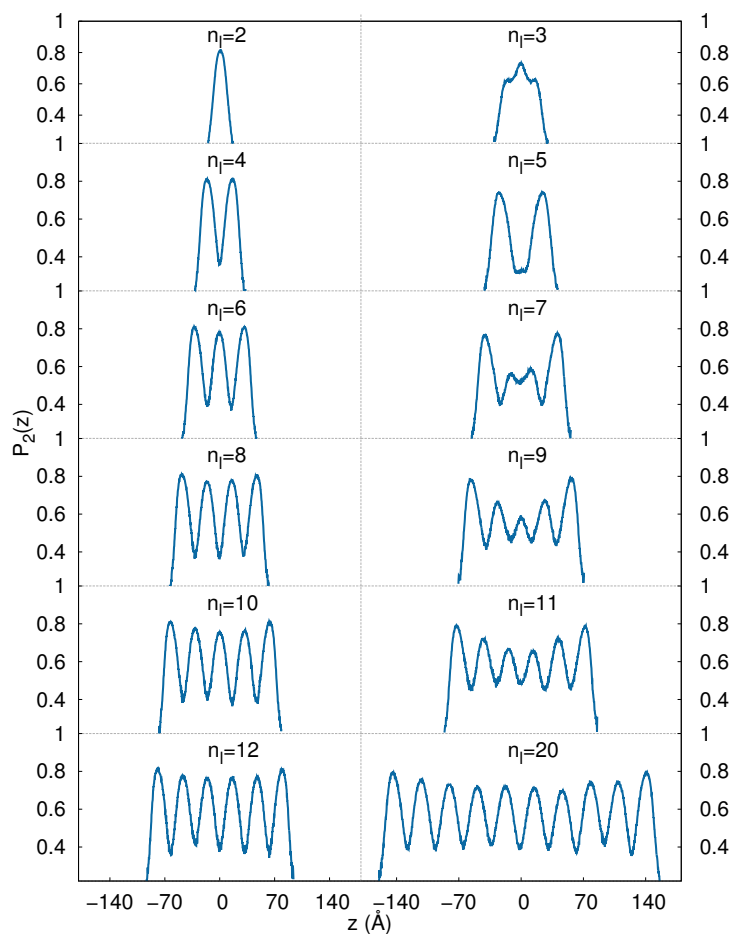


Fig. 7 Second rank order parameter $P_2(z)$ as a function of the position along the layer normal.

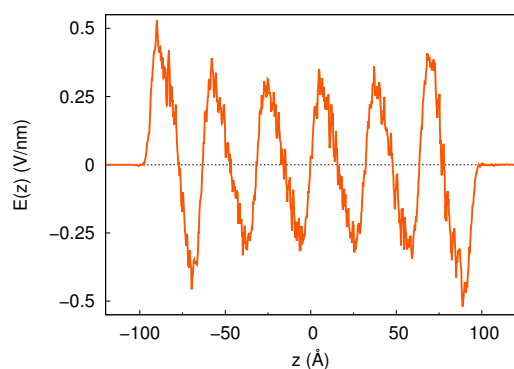


Fig. 9 Electric field $E(z)$ along z axis for the $n_l = 12$ sample.

be confirmed by plotting the electric field profile $E(z)$ along z axis (Figure 9), which can be obtained from the integration of Gauss's law in differential form $\nabla \cdot \vec{E} = \delta/\epsilon_0$:

$$E(z) = \frac{1}{\epsilon_0} \int_0^z \delta(z') dz' \quad (6)$$

where $\delta(z')$ is the linear charge density calculated from the simulation. Similarly to $P_1(z)$, $E(z)$ features peaks of opposite signs, as molecules of each sublayers are pointing in opposite directions. The extent of the oscillation though is sensibly higher at the two external interfaces, and it shows an enhanced asymmetry between peaks belonging to the same bilayer, revealing to the presence of a local net dipole. This net dipole is of course pointing in opposite directions for the top and bottom layers, so that the electric field and the electrostatic potential are zeroed outside the thin film, with no overall ferroelectricity³³.

3.3 Temperature dependence of the order in a 8CB thin film

The presence of an interface with vacuum (or air), besides leading to a higher positional and orientational order and inducing a homeotropic alignment of layers, exerts a major influence also on the transition temperatures of the LC phase. In fact, smectic films can also exist above the bulk smectic-nematic transition T_{SmN} close to an ordering surface, forming metastable systems called presmectic films^{58–60}. Such films maintain the layered structure typical of smectics, but the amplitude of density oscillations along the layer normal becomes much weaker toward the center of the film as temperature is increased. Another phenomenon peculiar to these systems is the so called thinning transition^{61–63}, consisting of a successive spontaneous layer-by-layer disruption occurring as the film is heated. Experiments show that for a certain temperature T there exists a maximum film thickness $n_l(T)$ above which the film thins spontaneously, whereas thinner films remain stable²⁷. Thinning transitions can be observed even below the bulk transition temperature if an external field perpendicular to the layer normal is applied to the film⁶⁴. It must be noted that in the case of 8CB, thinning temperatures cannot be experimentally determined for systems composed by less than ten layers. This is because the thinning temperature exceeds the nematic-isotropic liquid transition temperature, thus the meniscus, inevitably present in real films, melts and the formation of

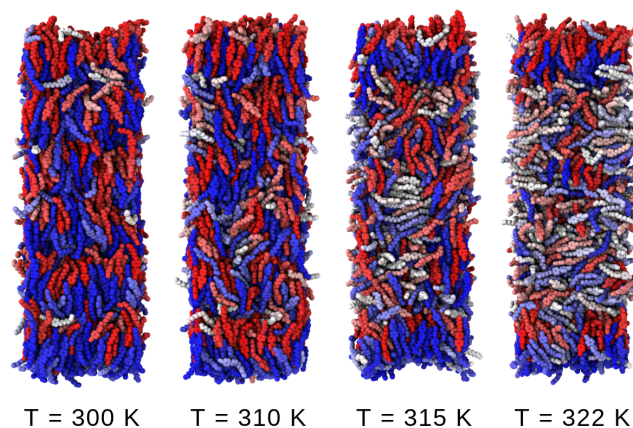


Fig. 11 Equilibrated configurations of the $n_l = 12$ film at various temperatures, showing smectic order of the interfacial layers even at $T=315, 322$ K, when the bulk 8CB is already in the isotropic phase.

droplets of isotropic liquid occurs, eventually leading to the film breakage³⁷.

Our system is much smaller and does not have a meniscus, but in order to verify whether it is able to reproduce any of the previous experimental observations, we ran a series of simulations on the six bilayer film by heating it progressively from 310 to 325 K. In Figure 10 (left) we report the corresponding density profile along the layer normal $\rho(z)$ as a function of temperature. It can be seen that as the sample is heated into the nematic temperature range (310–312.5 K), density oscillations decrease in the bulk of the sample, showing a loss of smectic order, while the bilayers on the surfaces remain well defined.

The temperature effect can be studied more in detail in Figure 10 (right) where we observe the trend of $\langle P_2 \rangle$ and of τ for each couple of bilayers: **internal (int)**, **central (cen)** and **external (ext) ones**. It can be noted that above 314 K the orientational order drops below 0.3, which is the threshold value below which we consider a sample as effectively isotropic. While the external bilayers experience only a slight loss of positional order as the temperature is increased, the internal and intermediate ones show a substantial decay of τ between 311 and 315 K. For the internal bilayers, the order parameter decreases much more quickly than for the intermediate ones, even though we cannot safely state that the system would undergo a layer-by-layer thinning transition, were the meniscus present. It is worth noting that even above 314 K, where we find a low value of orientational order parameter inside the film ($\langle P_2 \rangle < 0.4$), the τ of the external layers is still comparable with the one of the bulk sample.

The melting of the central layers, while the outside is still smectic, is apparent from Figure 11. This phenomenon is similar to what observed with the higher transition temperature in the outside layers in other systems, like the 4-n-butoxybenzylidene-4-n-octylaniline (4O.8) smectic⁶⁵. The simultaneous reduction of positional and orientational order might indicate the loss of nematic phase as a general trend for very thin films like the one studied in this work, although we cannot exclude then presence of the nematic phase in a very narrow temperature range.

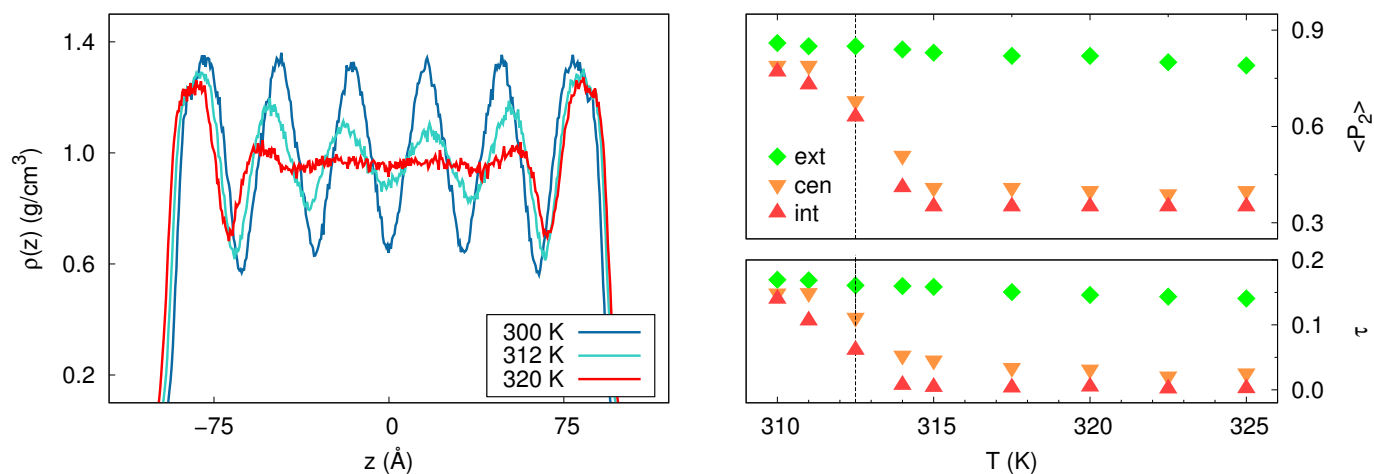


Fig. 10 On the left, density profiles of the $n_l = 12$ film along the z axis at 300, 312 and 320 K. On the right, nematic order parameter ($\langle P_2 \rangle$) and smectic order parameter τ for the **internal (int)**, **central (cen)** and **external (ext)** layer pairs as a function of temperature. The black vertical dashed line represents the T_{Nl} of the bulk sample.

3.4 Surface tension

In the bulk of a liquid, each molecule is attracted by its surrounding neighbours, resulting in a relatively strong cohesive force even in organic liquids. Conversely, molecules lying on the surface experience an unbalance of forces that usually leads to molecules to being pulled towards the bulk of the liquid. Thus, the system possesses a surface excess energy, defined as the free energy difference between the bulk sample and one with a surface exposed to a different phase. At constant temperature, volume, and number of particles, the surface tension γ can be defined as the partial derivative of the Helmholtz free energy F with respect to the surface area A :

$$\gamma = \left(\frac{\partial F}{\partial A} \right)_{T,V,N} \quad (7)$$

Since the average value of the potential energy for every system is known, obtaining a rough estimate of the surface tension from simulations is fairly straightforward if we make the approximation of neglecting entropic effects. In this limit, surface free energies can be simply calculated as the difference between the average potential energy of each film U_{film} and the one of the bulk U_{bulk} (here equal to 53 kcal/mol per molecule at 300 K and 1 atm). The ratio between such excess energy and twice the film surface area (since free standing films have two interfaces with the vacuum) returns the surface tension:

$$\gamma \approx \frac{U_{film} - U_{bulk}}{2L^2} \quad (8)$$

In Table 3, the values of the potential energy for systems with different number of layers n_l are reported. The film with $n_l = 2$ has a higher value of potential energy compared to the other even n_l samples, therefore suggesting that it may be more unstable. This observation is in agreement with the fact that the thinnest film which can be prepared experimentally is at least two bilayers thick⁶⁶ i.e. with $n_l = 4$. It can be seen in Table 3 that, in particular for samples with odd n_l , the potential energy of the system

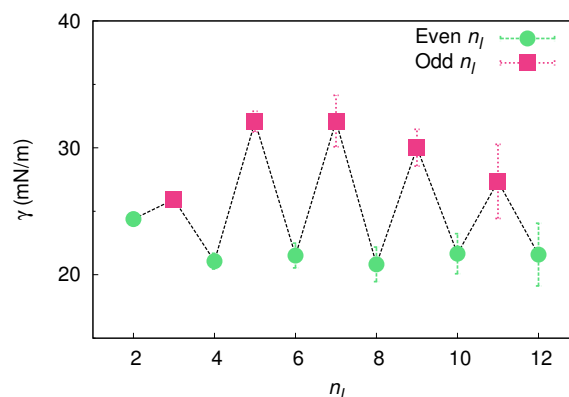


Fig. 12 Surface tension values γ as a function of the number of theoretical layers n_l for $N=1500$ samples and their error, computed employing the blocking average method⁶⁷.

decreases as the number of layers increases. In Figure 12, the trend of the surface tension is reported for both samples with even and odd n_l . It can be observed that simulated samples possessing an odd n_l show a higher surface tension, even if a comparison with experiment cannot be performed due to the impossibility of preparing stable films with odd n_l . In real systems this is due to the preparation method²⁷ and the presence of menisci³⁸, which act as a buffer for the excess/lack of molecules created when trying to arbitrary set the surface/volume ratio, i.e. to extend or reduce the thickness of the film in a continuous manner.

Experimental measurements have shown that for thin films with n_l up to 200 the surface tension can be considered constant with respect to the thickness²⁷. Also the surface tension of simulated systems with even n_l shows a constant trend, with an average value of 22 ± 1 mN/m. This is not too far from experimental measurements, which range from 24 to 30.9 mN/m depending on the technique^{36,68–71}. It should also be considered that entropic effects, which are not included in our evaluation of the surface

Table 3 Number of molecules N , calculated number of layers n_l , cell width L , excess potential energy per molecule of the film with respect to the bulk U_s , surface tension γ and average order parameter $\langle P_2 \rangle$.

N	n_l	$L(\text{\AA})$	U_s (kcal/mol)	$\gamma(mN/m)$	$\langle P_2 \rangle$
1500	2	152	1.08 ± 0.01	24.4 ± 0.3	0.65 ± 0.01
-	3	124	0.76 ± 0.01	25.9 ± 0.5	0.61 ± 0.02
-	4	107	0.46 ± 0.01	21 ± 1	0.65 ± 0.01
-	5	96	0.57 ± 0.01	32 ± 1	0.56 ± 0.02
-	6	88	0.32 ± 0.01	22 ± 1	0.65 ± 0.02
-	7	81	0.40 ± 0.03	32 ± 2	0.59 ± 0.02
-	8	76	0.23 ± 0.02	21 ± 1	0.64 ± 0.02
-	9	72	0.30 ± 0.01	30 ± 1	0.61 ± 0.02
-	10	68	0.19 ± 0.01	22 ± 2	0.64 ± 0.02
-	11	65	0.22 ± 0.02	27 ± 3	0.61 ± 0.02
-	12	62	0.16 ± 0.02	22 ± 2	0.64 ± 0.02
12000	20	136	0.13 ± 0.01	29 ± 3	0.61 ± 0.01

tension, should increase the actual value of the simulated γ , as the interface with vacuum is more ordered than the bulk 8CB (vide infra). It turns out that samples featuring an odd n_l possess a higher value of γ than those with even n_l but, as mentioned above, we expect such difference to decrease as systems with a high n_l are progressively considered. A special reference must be made again for the sample with $n_l = 3$, for which we observe a value of γ lower than expected. Differently from all the other films with an odd n_l , where the excess of molecules promotes the onset of $(n_l + 1)/2$ bilayers, in this system no inner layers can form and thus we observe two coexisting regions with one and two bilayers, respectively (see snapshot in Figure 3). This coexistence apparently contributes to lower the overall potential energy of the sample, resulting then in a lower value of surface tension.

4 Conclusions

We have provided a detailed atomistic simulation study of a freely suspended smectic thin film of 8CB, showing that MD can be a viable technique to investigate these quasi 2D systems. We have studied 8CB nano-thick films by varying the surface area and fixing the total number of molecules in order to obtain samples featuring in principle either an odd or an even number of theoretical layers. We have found that, as for real experiments both in the bulk and in thin films, 8CB molecules self-assemble in antiparallel bilayers, making this bilayer the natural unit of film thickness. In the case of odd n_l , we observed that if the number of molecules is intermediate between the optimal one for forming $(n_l - 1)/2$ and $(n_l + 1)/2$ bilayers, $(n_l + 1)/2$ bilayers are found, with a substantial increase of the surface tension and a decrease of the order in the inner layers. In the case of $n_l = 3$, where no inner bilayers can form, regions with one and two layers coexist. This difficulty to develop single monolayers rather than bilayers is consistent with and provides an explanation of the experimental observation of lack of ferroelectricity in very thin 8CB smectic films³³, that would be expected if an odd layer out could form. As for the surface tension, we find values fairly similar to the experimental ones for bulk 8CB. We also found that the bilayers at the interface with vacuum always have a higher positional and orientational order, and the largest spacing with respect to the bulk, while inner layers are only weakly influenced. We have determined the

characteristic propagation length of the surface-induced ordering, finding it to be of about 3 nm. The surface-induced order translates also in an increased temperature stability of the smectic phase for the outside layers, with the innermost portion of the sample becoming isotropic before the outer ones upon heating.

5 Acknowledgments

We thank Emilia-Romagna region for a Spinner Ph.D. fellowship granted to M.F.P. and CINECA Supercomputing Center for providing computer time through the ISCRA scheme (project FreeF). L. M. acknowledges funding by the French national grant ANR-10-LABX-0042-AMADEus, managed by the National Research Agency under the initiative of excellence IdEx Bordeaux programme (reference ANR-10-IDEX-0003-02).

References

- P. D. Gennes and J. Prost, *The physics of liquid crystals*, Clarendon press Oxford, 1993, vol. 23.
- J. M. Kosterlitz and D. J. Thouless, *J. Phys. C: Solid State Phys*, 1973, **6**, 1181.
- B. Halperin and D. Nelson, *Phys. Rev. Lett.*, 1978, **41**, 121–124.
- B. Halperin, *Symmetries and broken symmetries in condensed matter physics*, IDSET, 1981, pp. 183–195.
- L. D. Landau and E. M. Lifshitz, *Statistical Physics. Part 1*, Pergamon Press, Oxford, 1980.
- A. Pizzirusso, M. Savini, L. Muccioli and C. Zannoni, *J. Mater. Chem.*, 2011, **21**, 125–133.
- Y. Olivier, L. Muccioli and C. Zannoni, *ChemPhysChem*, 2014, **15**, 1345–1355.
- D. Moncton, R. Pindak, S. Davey and G. Brown, *Phys. Rev. Lett.*, 1982, **49**, 1865–1868.
- R. Berardi, L. Muccioli and C. Zannoni, *ChemPhysChem*, 2004, **5**, 104–111.
- G. Tiberio, L. Muccioli, R. Berardi and C. Zannoni, *ChemPhysChem*, 2009, **10**, 125–136.
- M. F. Palermo, A. Pizzirusso, L. Muccioli and C. Zannoni, *J. Phys. Chem*, 2013, **138**, 204901–204916.
- G. Gray, *Molecular structure and the properties of liquid crys-*

- tals, Academic Press, 1962.
- 13 T. Kato, C. Jin, F. Kaneuchi and T. Uryu, *Bull. Chem. Soc. Jpn.*, 1993, **66**, 3581–3584.
- 14 R. Berardi, M. Fehervari and C. Zannoni, *Mol. Phys.*, 1999, **97**, 1173–1184.
- 15 R. Dabrowski, J. Janik, J. Janik and K. Otnes, *Liq. Cryst.*, 1988, **3**, 443–452.
- 16 S. Urban, J. Przedmojski and J. Czub, *Liq. Cryst.*, 2005, **32**, 619–624.
- 17 A. J. Leadbetter, J. C. Frost, J. P. Gaughan, G. W. Gray and A. Mosley, *J. Phys. France*, 1979, **40**, 375–380.
- 18 A. J. McDonald and S. Hanna, *J. Chem. Phys.*, 2006, **124**, 164906.
- 19 L. D. Gaetani and G. Prampolini, *Soft Matter*, 2009, **5**, 3517–3526.
- 20 J. Zhang, J. Su and H. Guo, *J. Phys. Chem. B*, 2011, **115**, 2214–27.
- 21 T. Krentsel, O. Lavrentovich and S. Kumar, *Mol. Cryst. Liq. Cryst.*, 1997, **304**, 463–469.
- 22 S. V. Dvinskikh, I. Furó, H. Zimmermann and A. Maliniak, *Phys. Rev. E*, 2002, **65**, 061701.
- 23 B. Schulz, M. G. Mazza and C. Bahr, *Phys. Rev. E*, 2014, **90**, 040501.
- 24 G. Kruger, H. Spiessacke and R. Steenwinkel, *J. Phys. Colloques*, 1976, **37**, 123–126.
- 25 M. Cifelli and C. A. Veracini, *Phys. Chem. Chem. Phys.*, 2005, **7**, 3412–3415.
- 26 R. Pindak and D. Moncton, *Physics Today*, 1982, **35**, 57–62.
- 27 P. Oswald and P. Pieranski, *Smectic and columnar liquid crystals: concepts and physical properties illustrated by experiments*, Taylor & Francis, 2005.
- 28 C. Y. Young, R. Pindak, N. A. Clark and R. B. Meyer, *Phys. Rev. Lett.*, 1978, **40**, 773–776.
- 29 C. Bohley and R. Stannarius, *Soft Matter*, 2008, **4**, 683–702.
- 30 A. Becker and H. Stegemeyer, *Berichte der Bunsen Gesellschaft- Phys. Chem.*, 1997, **101**, 1957–1959.
- 31 C. Bahr, C. Booth, D. Fliegner and J. Goodby, *Phys. Rev. E*, 1995, **52**, R4612–R4615.
- 32 A. Eremin, S. Baumgarten, K. Harth, R. Stannarius, Z. Nguyen, A. Goldfain, C. Park, J. Maclennan, M. Glaser and N. Clark, *Phys. Rev. Lett.*, 2011, **107**, 268301.
- 33 H. Hsiung and Y. Shen, *Phys. Rev. A*, 1986, **34**, 4303–4309.
- 34 C. Bahr and D. Fliegner, *Berichte der Bunsen Gesellschaft- Phys. Chem.*, 1993, **97**, 1381–1386.
- 35 C. Biensan, B. Desbat and J. Turlet, *Thin Solid Films*, 1996, **285**, 293–296.
- 36 F. Schneider, *Rev. Sci. Instrum.*, 2002, **73**, 114–118.
- 37 F. Picano, P. Oswald and E. Kats, *Phys. Rev. E*, 2001, **63**, 021705.
- 38 K. Harth, B. Schulz, C. Bahr and R. Stannarius, *Soft Matter*, 2011, **7**, 7103–7111.
- 39 S. Dölle and R. Stannarius, *Langmuir*, 2015, **31**, 6479–6486.
- 40 B. M. Ocko, *Phys. Rev. Lett.*, 1990, **64**, 2160–2163.
- 41 Z. Qi, Z. H. Nguyen, C. S. Park, M. A. Glaser, J. E. Maclennan, N. A. Clark, T. Kuriabova and T. R. Powers, *Phys. Rev. Lett.*, 2014, **113**, 128304.
- 42 G. Watanabe, J.-I. Saito, N. Kato and Y. Tabe, *J. Chem. Phys.*, 2011, **134**, 054513.
- 43 G. Watanabe, J.-I. Saito, Y. Fujita and Y. Tabe, *J. Phys. Soc. Jpn*, 2013, **82**, 084603.
- 44 N. Matsuhashi, M. Kimura, T. Akahane and M. Yoshida, *AZojomo*, 2007, **3**, 1–9.
- 45 W. D. Cornell, P. Cieplak, C. I. Bayly, I. R. Gould, K. M. Merz, D. M. Ferguson, D. C. Spellmeyer, T. Fox, J. W. Caldwell and P. A. Kollman, *J. Am. Chem. Soc.*, 1995, **117**, 5179–5197.
- 46 J. Wang, P. Cieplak and P. A. Kollman, *J. Comput. Chem.*, 2000, **21**, 1049–1074.
- 47 J. C. Phillips, R. Braun, W. Wang, J. Gumbart, E. Tajkhorshid, E. Villa, C. Chipot, R. D. Skeel, L. Kale and K. Schulten, *J. Comput. Chem.*, 2005, **26**, 1781–1802.
- 48 D. Fincham and D. Heyes, *Adv. in Chemical Physics*, 1985, **63**, 493–575.
- 49 P. Hunenberger, *Adv. Polym. Science*, 2005, **173**, 105–147.
- 50 U. Essmann, L. Perera, M. L. Berkowitz, T. A. Darden, H. Lee and L. G. Pedersen, *J. Chem. Phys.*, 1995, **103**, 8577–8593.
- 51 W. L. McMillan, *Phys. Rev. A*, 1971, **4**, 1238–1246.
- 52 R. G. Marguta, E. M. del Río and E. de Miguel, *J. Phys.: Condens. Matter*, 2006, **18**, 10335–10351.
- 53 B. D. Swanson, H. Stragier, D. J. Tweet and L. B. Sorensen, *Phys. Rev. Lett.*, 1989, **62**, 909–912.
- 54 O. M. Roscioni, L. Muccioli, R. G. D. Valle, A. Pizzirusso, M. Ricci and C. Zannoni, *Langmuir*, 2013, **29**, 8950–8958.
- 55 A. Pizzirusso, R. Berardi, L. Muccioli, M. Ricci and C. Zannoni, *Chem. Sci.*, 2012, **3**, 573–579.
- 56 M. Fukuto, O. Gang, K. J. Alvine, B. M. Ocko and P. S. Pershan, *Phys. Rev. E*, 2008, **77**, 031607.
- 57 D. Frenkel and B. Smit, in *Understanding Molecular Simulations: From Algorithms to Applications.*, Accademic Press, San Diego, 1996.
- 58 P. G. De Gennes, *Langmuir*, 1990, **6**, 1448–1450.
- 59 G. Carbone, R. Barberi, I. Musevic and U. Krzic, *Phys. Rev. E*, 2005, **71**, 051704.
- 60 P. Ziherl, M. Vilfan, N. Vrbancic-Kopac, S. Zumer, R. Ondris-Crawford and G. Crawford, *Phys. Rev. E*, 2000, **61**, 2792–2798.
- 61 W. H. de Jeu, *Rev. Mod. Phys.*, 2003, **75**, 181–235.
- 62 T. Stoebe, P. Mach and C. C. Huang, *Phys. Rev. Lett.*, 1994, **73**, 3587–3590.
- 63 T. Kranjc and S. Zumer, *J. Chem. Phys.*, 1996, **105**, 5242–5245.
- 64 M. S. S. Pereira, M. L. Lyra and I. de Oliveira, *Phys. Rev. Lett.*, 2009, **103**, 177801.
- 65 A. Fera, B. Ostrovskii, D. Sentenac, I. Samoilenko and W. de Jeu, *Phys. Rev. E*, 1999, **60**, R5033–R5036.
- 66 T. Stoebe, P. Mach and C. C. Huang, *Phys. Rev. E*, 1994, **49**, 3587–3590.

- 67 H. Flyvbjerg and H. G. Petersen, *J. Chem. Phys.*, 1989, **91**, year.
- 68 R. Stannarius and C. Cramer, *Europhys. Lett.*, 1998, **42**, 43–48.
- 69 M. Eberhardt and R. B. Meyer, *Rev. Sci. Instrum.*, 1996, **67**, 2846–2851.
- 70 H. Schüring, C. Thieme and R. Stannarius, *Liq. Cryst.*, 2001, **28**, 241–252.
- 71 M. Tintaru, R. Moldovan, T. Belca and S. Frunza, *Liq. Cryst.*, 2001, **28**, 793–797.